Pattern Recognition 63 (2017) 87–101

Contents lists available at ScienceDirect

Pattern Recognition

journal homepage: www.elsevier.com/locate/pr

Dense registration of fingerprints

Xuanbin Si [a], Jianjiang Feng [b,*], Bo Yuan [a], Jie Zhou [b]

[a] Graduate School at Shenzhen, Tsinghua University, Shenzhen 518055, China
[b] Tsinghua National Laboratory for Information Science and Technology (TNList), Department of Automation, Tsinghua University, Beijing 100084, China

ARTICLE INFO

Article history:
Received 1 February 2016
Received in revised form
5 July 2016
Accepted 19 September 2016
Available online 21 September 2016

Keywords:
Fingerprint
Distortion
Registration
Dense correspondence
MRF

ABSTRACT

Dense registration of different impressions of the same finger is beneficial to various fingerprint matching methods. This is a challenging problem due to elastic distortion of finger skin and sparsity of distinctive features (namely minutiae) in fingerprints. Most existing fingerprint registration algorithms produce only correspondences between minutiae, which are not sufficient for dense registration of fingerprints. In this paper, we proposed a novel dense fingerprint registration algorithm, which consists of a composite initial registration step and a dual-resolution block-based registration step. The dual-resolution block-based registration is approached in an energy minimization framework which consists of local search, energy function construction and global optimization. In local search step, a candidate set of transformations of every input image block are found using image correlation w.r.t. the corresponding reference image block. In energy function construction, two factors are considered: (1) the similarity between the transformed input block and the corresponding reference block, and (2) the compatibility between transformations of neighboring input blocks. In global optimization, a region growing style algorithm is proposed to minimize the energy function. Experimental results on three databases containing many distorted fingerprints, namely FVC2004 DB1, Tsinghua Distorted Fingerprint database and NIST SD27 latent fingerprint database, show that the proposed algorithm not only produces more accurate registration results but also improves the matching performance by fusion of minutiae matching and image correlation.

1. Introduction

Although automatic fingerprint recognition technology has been widely used in various applications, there is still large room for improvement of matching accuracy, especially in the case of low quality fingerprints [1]. Degradation of fingerprint quality can be photometric or geometrical. Photometric degradation can be caused by non-ideal skin conditions and background noise. Geometrical degradation is mainly caused by skin distortion. Photometric degradation has been widely studied and a number of enhancement algorithms [2–6] have been proposed. On the contrary, geometrical degradation due to skin distortion has not yet received sufficient attention, despite of the importance of this problem.

Elastic distortion is introduced due to the inherent flexibility of fingertips, contact-based fingerprint acquisition procedure, and a purposely lateral force or torque, etc [7,8]. Skin distortion increases the intra-class variations, namely the difference among fingerprints from the same finger. Although distortion affects all fingerprint matching methods, image-based matchers are much more sensitive to distortion than minutiae-based matchers. This is one of the reasons for the popularity of minutiae-based matchers. However, the performance of minutiae matchers may drastically drop when the distortion is severe, the number of genuine minutiae is small, or many spurious minutiae are present.

In order to overcome the limitation of minutiae-based matching, researchers have proposed to use some extended features, such as ridge orientation field [9], ridge period map [10,11], and ridge skeleton [12,13] etc. Although these methods improve the discriminating ability of minutiae matchers, they also suffer from distortion.

In order to remove the negative impact of distortion, it is necessary to estimate a dense deformation field between two fingerprints. “Dense” means that it can align not only minutiae but also ridges. This is a deformable image registration problem, which is a popular topic in medical image analysis [14], but is first proposed in the fingerprint recognition community. The proposed dense registration algorithm combines the advantages of minutiae-based matching and image-based matching, and overcomes their disadvantages. It can densely register two fingerprints. It is based on a composite initial registration step and a dual-resolution

* Corresponding author.
E-mail addresses: sixuanbin@sz.tsinghua.edu.cn (X. Si), jfeng@tsinghua.edu.cn (J. Feng), yuanb@sz.tsinghua.edu.cn (B. Yuan), jzhou@tsinghua.edu.cn (J. Zhou).

http://dx.doi.org/10.1016/j.patcog.2016.09.012
0031-3203/

block-based registration step. In initial registration step, the minutiae-based matching can decrease the distortion in global level using the TPS model, which overcomes the disadvantage of image-based matching which cannot handle distortion in global level. In dual-resolution block-based registration step, the idea is to find dense point correspondences between two initial registered fingerprints using local image-based matching. Since the points are regularly sampled grid points, it is not restricted by the sparsity of minutiae. Combining the advantage of minutiae-based matching which can decrease the distortion in global level and the advantage of local image-based matching which can well handel the distortion in local level, the proposed dense registration algorithm can register distorted fingerprints accurately. Registration results for a pair of distorted fingerprints are given in Fig. 1 to compare three different methods, namely, the minutiae-based rigid transformation, the minutiae-based TPS model, and the proposed dense registration method.

The flowchart of the proposed registration algorithm is shown in Fig. 2. Initialized by a minutiae-based registration algorithm, a dual-resolution block matching algorithm is proposed to find dense correspondences between an input fingerprint and a reference fingerprint. Block matching is approached in an energy minimization framework which consists of local search, energy function construction and global optimization. In local search step, a candidate set of transformations of every input image block, which lead to good alignment between the input image block and the reference fingerprint, are found. In energy function construction, due to the continuity of deformation field, two factors are considered: (1) the similarity between the transformed input block and the corresponding reference block, and (2) the compatibility between transformations of neighboring input blocks. In global optimization, a region growing style algorithm is proposed to minimize the energy function. Benefitting from the way to construct energy function and its optimization algorithm, the dual-resolution block-based registration is insensitive to inaccurate initialization and robust to noise.

The proposed algorithm has been evaluated on three databases which contain many distorted fingerprints, namely FVC2004 DB1 [15], Tsinghua Distorted Fingerprint (TDF) database and NIST SD27 latent fingerprint database [16]. Not only the registration accuracy but also matching accuracy are evaluated on these three databases. In order to measure registration accuracy, we have manually registered 120 pairs of distorted fingerprints in TDF as ground truth using a specially designed registration software tool. To quantitatively evaluate the contribution of the proposed dense registration algorithm to matching performance, we conduct matching experiments on fingerprints without/with dense registration. All experimental results demonstrate that the proposed algorithm not only produces more accurate registration results but also improves the matching performance significantly by fusion of minutiae

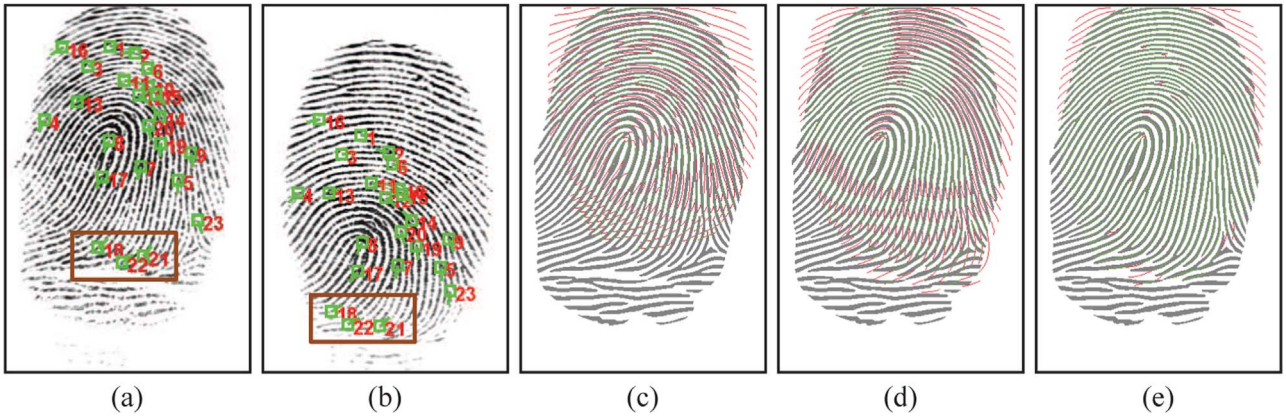

Fig. 1. Registration results for a pair of distorted fingerprints from FVC2004 DB1. (a) Reference fingerprint, (b) input fingerprint, (c) fingerprints aligned by the minutiae-based rigid transformation model, (d) fingerprints aligned by the minutiae-based TPS model, and (e) fingerprints aligned by the proposed dense registration algorithm. The matched minutiae pairs are shown on the reference and input fingerprints. Ridge skeletons of the registered input fingerprint are overlaid on the binarized reference fingerprint to visualize the registration result. The well registered skeletons are illustrated as green lines, while the others are illustrated as red lines. Due to distortion of the input fingerprint, the minutiae-based rigid registration fails to align the ridges everywhere, the minutiae-based TPS registration is good in the area with many correctly matched minutiae, but fails in the other area. Also, due to three pairs of wrong matched minutiae (contained in the brown boxes), the minutiae-based TPS registration totally fails to align the ridges in the bottom area. The proposed dense registration algorithm obtains good registration result for areas without matched minutiae and is insensitive to wrongly matched minutiae. (For interpretation of the references to color in this figure legend, the reader is referred to the web version of this article.)

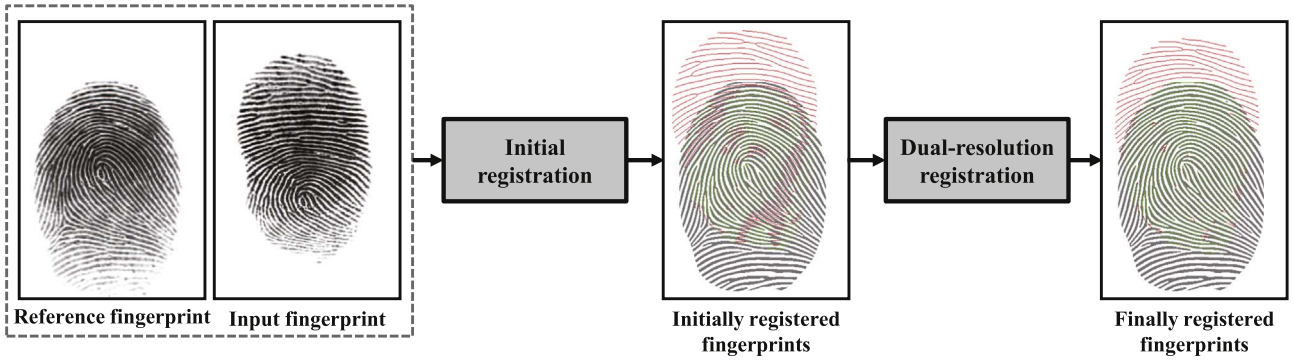

Fig. 2. Flowchart of the proposed registration algorithm. Given a pair of fingerprints, two registration steps (namely, initial registration and dual-resolution registration) are performed to align the two fingerprints densely.

matching and image correlation.

The rest of the paper is organized as follows. In Section 2, we review the related work. In Sections 3 and 4, we present the proposed registration algorithm in details. In Section 5, we give the experiment results. In Section 6, we summarize the paper and discuss the future research directions.

2. Related work

For a fingerprint registration algorithm, a transformation model is used to register input fingerprint to reference fingerprint. The most common transformation model is the rigid transformation model which contains translation and/or rotation [9,17]. However, it is obvious that the rigid transformation model cannot handle distorted fingerprints. Thus, some researchers proposed to use more powerful transformation models, such as thin-plate spline (TPS) model [18,19], to register two fingerprints. However, the success of TPS-based registration relies on a large number of correctly matched points. Matched minutiae outputted by minutiae matching algorithms [17,11,20,21] are usually unreliable when fingerprints contain severe distortion. Even if the matched minutiae are all correct, the TPS model derived from the matched minutiae cannot densely register distorted fingerprints due to the sparsity of minutiae. Although ridge matching algorithms [12,13] may produce more matching points, the ridge correspondences are incorrect when there exist wrongly matched minutiae or there are topological changes in ridge skeletons due to noise.

Different from the existing methods, our method can find dense point correspondence between two fingerprints. It consists of an initial registration step and a dual-resolution block-based registration step. By using initial registration, we can greatly reduce the search space and then markedly save the computation time. By using dual resolution block based registration, we can further obtain the better registration accuracy. The details about these two steps will be described in the next two sections.

3. Initial registration

In the initial registration step, a minutiae matching algorithm is used to find matched minutiae between the input and reference fingerprints. If the number of matched minutiae exceeds a threshold t_n, a TPS model [22] fitted to the matched minutiae is used to initially register the input fingerprint to the reference fingerprint. Otherwise, more robust features (orientation map and period map) are used to estimate the rigid transformation between two fingerprints. The later method is mainly useful for a few cases where the common area of two fingerprints is very small.

3.1. Minutiae-based initial registration

VeriFinger 6.2 SDK [23] is used to extract minutiae from fingerprints. The spectral clustering method in [24], a powerful method to find consistent correspondences between two sets of features, is modified to find matching minutiae between two fingerprints. We chose this method because our experiments showed that it performs better in finding corresponding minutiae than several well known minutiae matching algorithms, such as VeriFinger SDK, relaxation based method in [20], greedy method in [17]. There are two major differences: (1) we eliminate minutiae pairs whose minutiae cylinder-code (MCC) descriptors [20] are too different, (2) the mapping constraints include the difference between the length of the line connecting two minutiae, the difference between the relative angle of two minutiae, and the difference between the relative angle of the line connecting two minutiae and one of the two minutiae. In order to set reasonable thresholds of these mapping constraints, we do some statistics on genuine matches of FVC2004 DB1_B and use the statistical results to set the thresholds.

3.2. Orientation & period-based initial registration

To register the ridge orientation and period maps of two fingerprints, which are estimated using the method in [2] (there are some other methods for estimating ridge orientation and period such as the methods in [25,26]), we do a full search of the space of rigid transformation parameters by maximizing the following objective function:

$$\underset{x,y,\psi}{\operatorname{argmax}} \| \operatorname{OrientDiff}\left(\boldsymbol{O}_R, \boldsymbol{O}_I(x,y,\psi)\right) \le \theta_t \ \&\operatorname{PeriodDiff}\left(\boldsymbol{P}_R, \boldsymbol{P}_I(x,y,\psi)\right) \le p_t \|_0, \quad (1)$$

where x and y denote the translation parameters, ψ denotes the rotation parameter, $\boldsymbol{O}_I$ is the orientation map of the input fingerprint, $\boldsymbol{O}_R$ is the orientation map of the reference fingerprint, $\boldsymbol{P}_I$ is the period map of the input fingerprint, $\boldsymbol{P}_R$ is the period map of the reference fingerprint, function OrientDiff() computes the difference of two orientation maps at each location, function PeriodDiff()

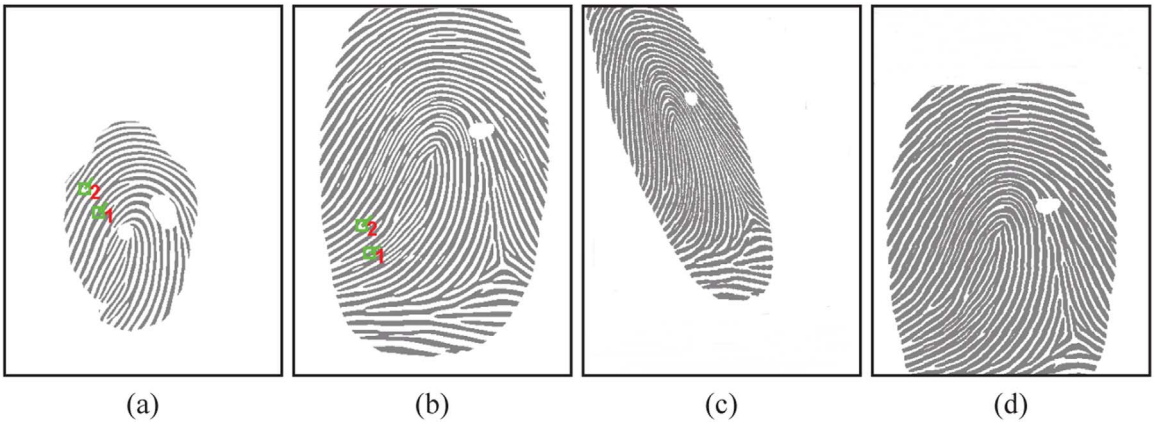

Fig. 3. An example for initial registration using orientation map and period map. (a) Reference fingerprint, (b) input fingerprint, (c) initially registered input fingerprint using the minutiae-based method, and (d) initially registered input fingerprint using the orientation & period-based method. The minutiae-based method fails to align the two fingerprints due to the incorrectly matched minutiae (marked in (a) and (b)) which are caused by noise and the small common area between two fingerprints. However, the orientation & period-based method is successful.

computes the difference of two period maps at each location, $\|\cdot\|_0$ counts the number of nonzero elements, θ_t and p_t are predefined orientation and period thresholds. Note that the ridge orientation map and period map are sampled on blocks of 8×8 pixels. Here, the block size is first selected based on experience and then tuned according to the experimental results of a few examples. Finally, we register the input fingerprint to the reference fingerprint using the obtained rigid transformation parameters.

The level 1 features (orientation map and period map) based registration method is more robust to noise than the minutiae-based registration method as shown in Fig. 3, where the minutiae-based registration is incorrect since the two matching minutiae pairs are wrong, but the orientation & period-based method is able to successfully register the two fingerprints. Successful fingerprint registration based on orientation field are also reported in a recent work [27].

4. Dual-resolution block-based registration

The proposed dual-resolution block-based registration consists of a TPS warping after a low resolution block matching step and a TPS warping after a high resolution block matching step. It is used to further register the input fingerprint to reference fingerprint accurately. The flowchart of dual-resolution block-based registration is shown in Fig. 4.

We define sampling grid on initially registered input fingerprint, and then find the optimal transformation of every sampling block using image correlation w.r.t. the corresponding reference block image. However, due to limited information of a single block, locally optimal transformation may not be the true transformation. Hence multiple candidate transformations are found to increase the probability of including the true one. In order to determine the globally optimal transformation for each input block, contextual information, namely compatibility between the transformations of neighboring input blocks, needs to be utilized. Thus we construct an energy function considering both the similarity between the transformed input block and the corresponding reference block and compatibility between transformations of neighboring input blocks. Finally, a global optimization step is performed to minimize the energy function, namely determining the globally optimal transformation for each input block. In the following subsections, we describe the three steps of the block matching algorithm: (1) local search, (2) energy function construction, and (3) global optimization.

4.1. Local search

The input fingerprint is divided into a set of blocks $\{\mathbf{\Gamma}_i\}$ which are overlapped only in boundary lines. The block size is 41×41/21×21 pixels in low/high resolution block matching (Note that the block sizes are first selected based on experience and then tuned according to the experimental results of a few examples). Then multiple candidate transformations of every input block are found using image correlation w.r.t. the corresponding region in the reference fingerprint. The flowchart of local search is shown in Fig. 5.

For the ith input block $\mathbf{\Gamma}_i$, we find multiple candidate transformation parameters, namely $\mathbf{\Upsilon}_i = \{\mathbf{\Upsilon}_{i,1}, \mathbf{\Upsilon}_{i,2}, \ldots, \mathbf{\Upsilon}_{i,n_c}\}$, under which the similarities with the corresponding areas in the reference fingerprint are high. Here, n_c denotes the length of candidate list, $\mathbf{\Upsilon}_{i,j} = (t_{x_{i,j}}, t_{y_{i,j}}, \alpha_{i,j}, s_{i,j})(1 \le j \le n_c)$, where $t_{x_{i,j}}$ and $t_{y_{i,j}}$ denote the translation parameters in x and y directions, $\alpha_{i,j}$ denotes the rotation parameter, $s_{i,j}$ denotes the scale parameter. Note that, only when both the foreground area ratio of $\mathbf{\Gamma}_i$ and the foreground area ratio of its search area $\boldsymbol{A}_i$ ($81 \times 81/41 \times 41$ pixels in low/high resolution block matching and the center point is the same to the one of $\mathbf{\Gamma}_i$) exceed threshold t_a, $\mathbf{\Gamma}_i$ is viewed as a valid block. We estimate transformation parameters only for valid blocks.

In order to find multiple candidate transformation parameters, a suitable search technique must be developed. We adopt image correlation as the similarity measure. The most straightforward search technique is to exhaustively try all possible parameters, i.e., do a full search. However, it is very time consuming. In order to improve efficiency, local ridge orientation and period are first used to markedly reduce the search scope of rotation and scale parameters, and then Fast Fourier Transform (FFT) is used to find two translation parameters.

For block $\mathbf{\Gamma}_i$, we sample the orientation and period maps using 5×5 regular grids and obtain the orientation vector $\boldsymbol{O}_{I_i}$ and period vector $\boldsymbol{P}_{I_i}$ on input block, and the orientation vector $\boldsymbol{O}_{R_i}$ and period vector $\boldsymbol{P}_{R_i}$ on reference block $\mathbf{\Phi}_i$ whose size and position are the same to $\mathbf{\Gamma}_i$. Further, we get the orientation difference vector $\mathbf{\Theta}_i = \boldsymbol{O}_{R_i} - \boldsymbol{O}_{I_i}$ and the period ratio vector $\mathbf{\Delta}_i = \boldsymbol{P}_{R_i} ./ \boldsymbol{P}_{I_i}$.

In order to set the search scope of rotation, we need to calculate the mean and coherence of $\mathbf{\Theta}_i$. The method described in [25,26] is used to calculate the mean of $\mathbf{\Theta}_i$:

$$\bar{\theta}_i = \frac{1}{2}\text{atan2}\left(\sum \sin(2\mathbf{\Theta}_i), \sum \cos(2\mathbf{\Theta}_i)\right), \tag{2}$$

where $\bar{\theta}_i$ denotes the mean of $\mathbf{\Theta}_i$. And orientation coherence method described in [25,26] is used to calculate the coherence of $\mathbf{\Theta}_i$:

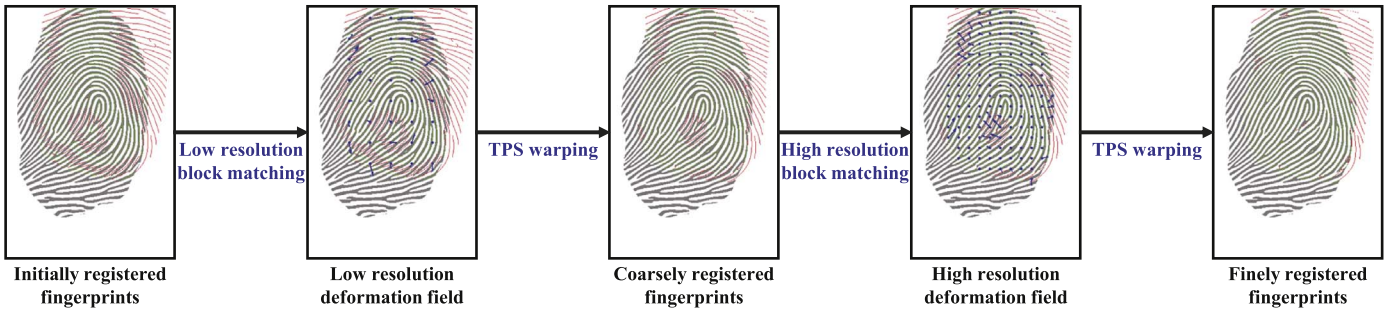

Fig. 4. Flowchart of dual-resolution block-based registration. Given the initially registered fingerprints, low resolution registration and high resolution block-based registration are performed to align the two fingerprints accurately. In low resolution and high resolution block-based registration, corresponding blocks of a set of sampling blocks (a larger sampling interval for low resolution registration and a smaller one for high resolution registration) in the input fingerprint are found and a TPS model fitted to the center points of matched blocks is used to align the two fingerprints. The blue dots illustrate the center points of valid blocks and the blue arrows illustrate their displacements. Note that, the lengths of blue arrows are trebled for visualization purpose. (For interpretation of the references to color in this figure legend, the reader is referred to the web version of this article.)

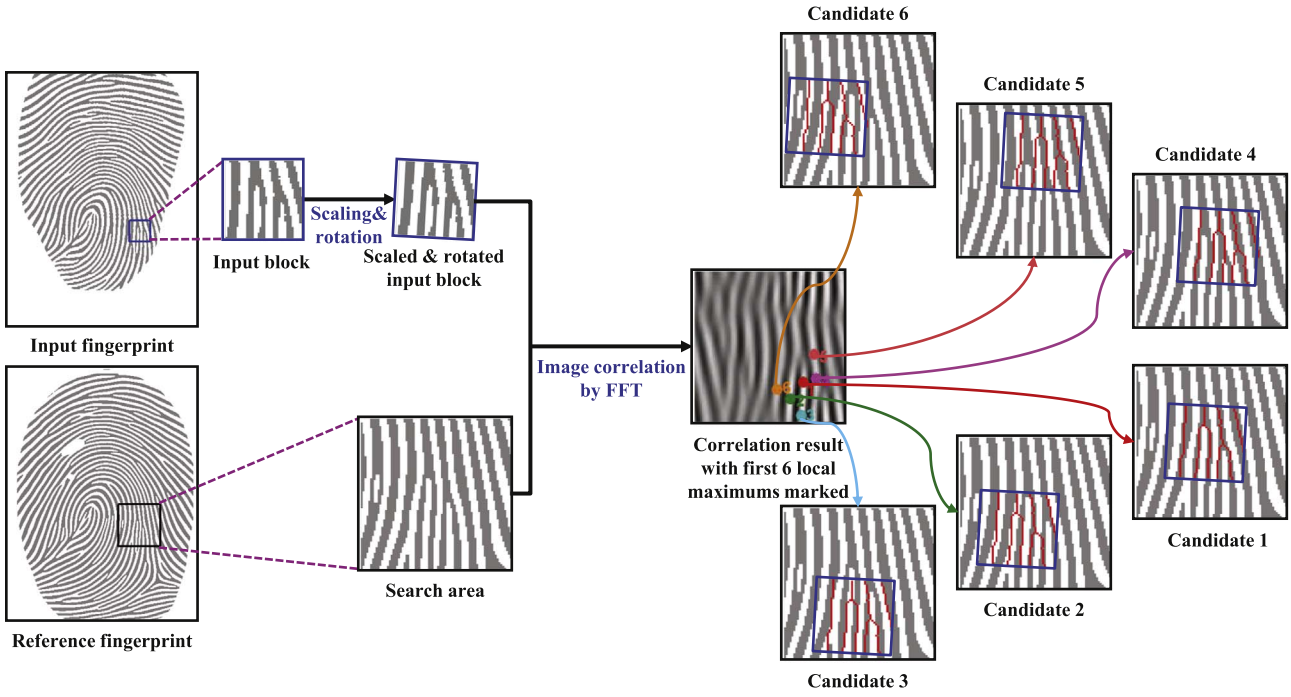

Fig. 5. Flowchart of local search. The input block is first transformed using rotation ($\frac{\pi}{60}$ in clockwise) and scaling (0.983) parameters estimated from local ridge orientation and period information (in this example, we use only one rotation parameter). Then image correlation is computed to find multiple candidate translation parameters. The scaled and rotated input blocks transformed with six candidate translation parameters are overlaid on search area and shown as red skeleton images for visualization purpose. (For interpretation of the references to color in this figure legend, the reader is referred to the web version of this article.)

$$\sigma_i = \frac{|(\sum \sin(2\Theta_i), \sum \cos(2\Theta_i))|}{\text{length}(\Theta_i)}, \tag{3}$$

where σ_i denotes the coherence, $|\cdot|$ calculates the norm of a vector, function length() calculates the length of a vector. Finally, the search scope of rotation is set as $[\bar{\theta}_i - (1-\sigma_i)\frac{\pi}{6}, \bar{\theta}_i + (1-\sigma_i)\frac{\pi}{6}]$. The scale factor is defined as:

$$s_i = \text{mean}(\Delta_i). \tag{4}$$

We transform block Γ_i using s_i and sampled rotation parameters from $[\bar{\theta}_i - (1-\sigma_i)\frac{\pi}{6}, \bar{\theta}_i + (1-\sigma_i)\frac{\pi}{6}]$, where the sampling interval is $\frac{\pi}{90}$. Then we rotate them by 180°, pad with zeros to create $(41+81)\times(41+81)/(21+41)\times(21+41)$ matrixes in low/high resolution block matching, do the FFT, and record the results as $\boldsymbol{F}_i = \{\boldsymbol{F}_{i,1}, \boldsymbol{F}_{i,2}, \ldots, \boldsymbol{F}_{i,\xi_i}\}$, where ξ_i denotes the sampling number of rotation parameters. At the same time, we pad the search area $\boldsymbol{A}_i$ with zeros to create $(81+41)\times(81+41)/(41+21)\times(41+21)$ matrixes in low/high resolution block matching, do the FFT, and record the result as $\boldsymbol{M}_i$. Next, we do the inverse FFT to $\boldsymbol{F}_{i,k}.*\boldsymbol{M}_i (1 \le k \le \xi_i)$ and obtain ξ_i correlation results. The first n_c local maximums in all ξ_i correlation results are found and denoted as $\tau_i = \{\tau_{i,1}, \tau_{i,2}, \ldots, \tau_{i,n_c}\}$ whose locations are used to calculate translation, rotation and scale parameters. Thus, we get n_c candidate transformations $\Upsilon_i = \{\Upsilon_{i,1}, \Upsilon_{i,2}, \ldots, \Upsilon_{i,n_c}\}$, where $\Upsilon_{i,j} = (t_{x_{i,j}}, t_{y_{i,j}}, \alpha_{i,j}, s_{i,j})(1 \le j \le n_c)$.

4.2. Energy function construction

After local search, we obtain a list of n_c candidate transformations, $\Upsilon_i = \{\Upsilon_{i,1}, \Upsilon_{i,2}, \ldots, \Upsilon_{i,n_c}\}$, for block Γ_i. We need to choose the optimal transformation for block Γ_i.

We address this problem by searching for a set of candidates, $\mathbf{r}^*$, which minimizes an energy function $E(\mathbf{r})$. Let r_i denotes the index of the selected candidate for block Γ_i, and $\mathbf{r} = \{r_1, r_2, \ldots, r_{n_p}\}$ be the vector of the indices of the selected candidates for all n_p valid blocks. The solution space for $\mathbf{r}$ is all possible combinations of candidate indices, which is very large. The choice of a proper energy function is crucial for the success of this method. We consider two factors in designing the energy function: (1) the similarity between the transformed input block and the corresponding reference block, and (2) the compatibility between transformations of neighboring input blocks.

The energy function is defined as

$$E(\mathbf{r}) = E_s(\mathbf{r}) + w_c E_c(\mathbf{r}), \tag{5}$$

where $E_s(\mathbf{r})$ denotes the similarity term, $E_c(\mathbf{r})$ denotes the compatibility term, and w_c is the weight of compatibility term. The similarity term is defined as

$$E_s(\mathbf{r}) = \sum_{i=1}^{n_p} \exp(-\tau_{i,r_i}/\mu_1), \tag{6}$$

where μ_1 is a harmonic factor. The compatibility term is defined as

$$E_c(\mathbf{r}) = \sum_{(i,j)\in\mathcal{N}} \left(1 - C(\Upsilon_{i,r_i}, \Upsilon_{j,r_j})\right), \tag{7}$$

where $\mathcal{N}$ denotes the set of adjacent blocks which are 4-connected neighbors. The compatibility is defined as

$$C(\Upsilon_{i,r_i}, \Upsilon_{j,r_j}) = \frac{1}{2}\exp(-w_1 d_1^2/\mu_2) + \frac{1}{2}\exp(-w_2 d_2^2/\mu_2), \tag{8}$$

where d_1 and d_2 denote the distances of two corresponding vertexes between two neighboring input blocks transformed with Υ_{i,r_i} and Υ_{j,r_j}, μ_2 is a harmonic factor, w_1 and w_2 are penalty factors calculated using $w_1 = a + b|\sin(\phi_1)|$, $w_2 = a + b|\sin(\phi_2)|$. ϕ_1 and ϕ_2 denote the difference between the angles of the two lines connecting two corresponding vertexes and ridge orientation of reference fingerprint at the middle point of two corresponding vertexes, a and b denote two linear parameters. w_1 and w_2 mean that there is a large penalty when the displacement is large along

the direction normal to ridge orientation. The definition for compatibility is illustrated in Fig. 6. Two compatibility examples are given in Fig. 7.

4.3. Global optimization

The Energy function in Eq. (5) describes a Markov random field (MRF) problem. To minimize it, a region growing MRF optimization algorithm is developed. First, the beginning region (seed region) is selected. For a block in input fingerprint and the corresponding block in reference fingerprint, their image correlation coefficient is calculated using the following formula:

$$\kappa_i = \frac{\sum_j (\mathbf{\Gamma}_{i_j} - \bar{\mathbf{\Gamma}}_i)(\mathbf{\Phi}_{i_j} - \bar{\mathbf{\Phi}}_i)}{\sqrt{\left(\sum_j (\mathbf{\Gamma}_{i_j} - \bar{\mathbf{\Gamma}}_i)^2\right)\left(\sum_j (\mathbf{\Phi}_{i_j} - \bar{\mathbf{\Phi}}_i)^2\right)}}, \tag{9}$$

where κ_i denotes the image correlation coefficient between $\mathbf{\Gamma}_i$ and its reference block $\mathbf{\Phi}_i$ whose size and position are the same to $\mathbf{\Gamma}_i$, $\mathbf{\Gamma}_{i_j}$ and $\mathbf{\Phi}_{i_j}$ denotes the jth pixel value in foreground area of $\mathbf{\Gamma}_i$ and $\mathbf{\Phi}_i$, $\bar{\mathbf{\Gamma}}_i$ and $\bar{\mathbf{\Phi}}_i$ denotes the mean pixel value of foreground area of $\mathbf{\Gamma}_i$ and $\mathbf{\Phi}_i$. We find all valid blocks in input fingerprint if the corresponding image correlation coefficient exceeds the predetermined threshold t_r. The largest 4-connected region of these blocks is set as the beginning region. The blocks in beginning region are deemed as fixed blocks, namely their transformations have been

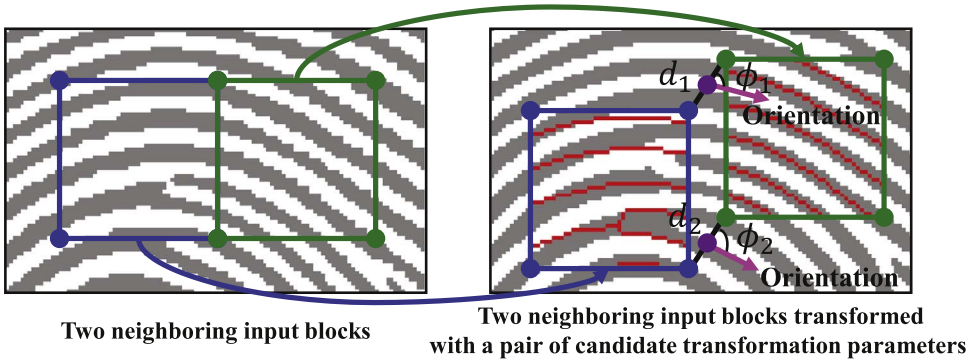

Fig. 6. Compatibility between two transformed neighboring blocks. The compatibility value is 0.222.

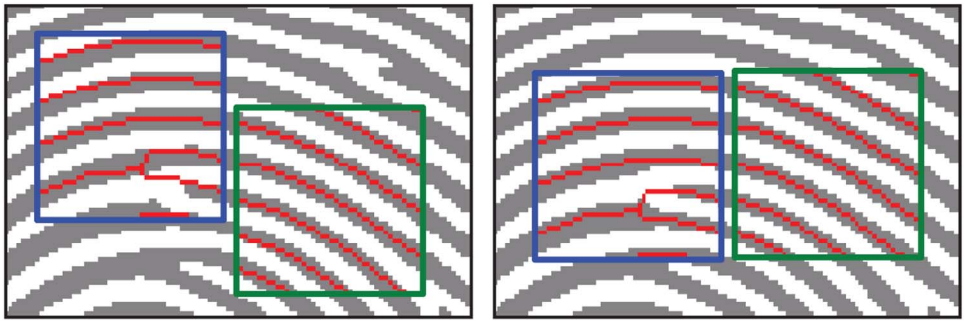

Fig. 7. (a) A pair of transformed neighboring blocks with low compatibility value (0.103) and (b) a pair of transformed neighboring blocks with high compatibility value (0.934).

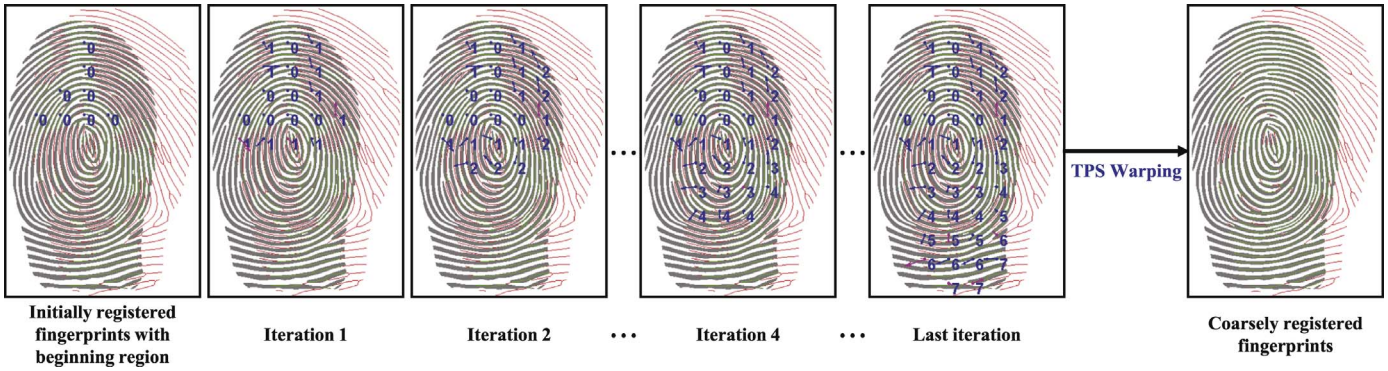

Fig. 8. The process of region growing MRF optimization (at low resolution). The first image shows the initially registered fingerprints and the last one shows the coarsely registered fingerprints. The blue numbers from 1 to 7 show the region growing order of blocks. The set of number 0 denotes the beginning region. The points and the arrows illustrate the center points of fixed and undetermined blocks and their displacements after current iteration. The magenta arrows indicate the blocks which are not fixed after current iteration, while the blue arrows indicate the blocks which are fixed after current iteration. Note that the lengths of arrows are trebled for visualization purpose. (For interpretation of the references to color in this figure legend, the reader is referred to the web version of this article.)

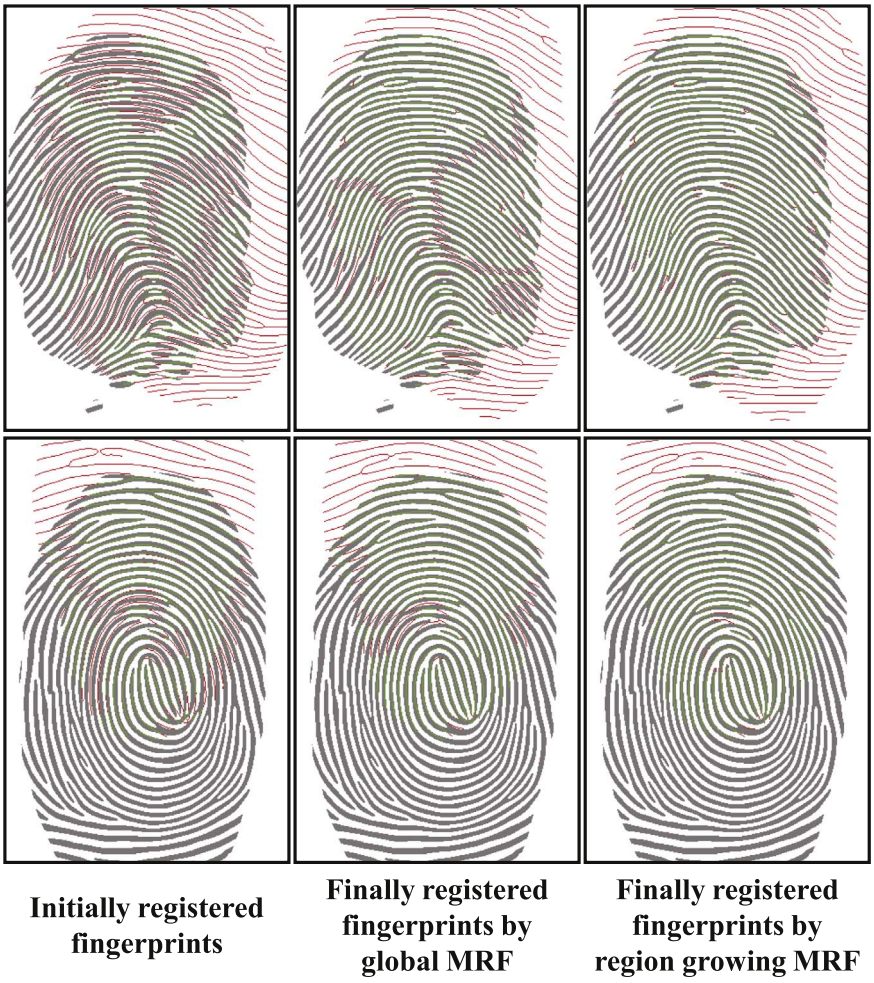

Fig. 9. Two examples showing the registration results of global MRF optimization algorithm and region growing MRF optimization algorithm. We can see that region growing algorithm obtains better results, with more well aligned ridge skeletons.

Table 1
Parameters used in our experiments.

Parameter (**s**)	**Description**	**Values** (**in initial or low/high resolution registration**)
t_n	threshold of the number of initially matched minutiae pairs	6
θ_t	predefined orientation threshold in orientation & period-based initial registration	$\frac{\pi}{18}$
p_t	predefined period threshold in orientation & period-based initial registration	1 pixel
t_a	foreground area ratio threshold	0.5/0.5
n_c	length of candidate list	6/6
w_c	weight of compatibility term	1/1
μ_1	harmonic factor in similarity term	$1 \times 10^7/0.5 \times 10^7$
μ_2	harmonic factor in compatibility term	200/100
a, b	linear parameters in penalty factor	0.5/0.5, 1/1
t_r	predefined correlation coefficient threshold in global optimization	0.4/0.5
t_s	similarity threshold in global optimization	0.74/0.83
t_c	compatibility threshold in global optimization	0.35/0.3
$\lambda_{c,1}$	compatibility weight between the fixed block and undetermined block	3/3
$\lambda_{c,2}$	compatibility weight between two undetermined blocks	1/1

Table 2
Fingerprint databases for evaluating the proposed algorithm.[a]

Database	**Description**	**Fingerprint size** (**width** $\times$ **high pixels**)	**Challenges**
FVC2004 DB1_A	800 fingerprints	640×480 pixels	large distortion, small area, dry or wet finger
TDF	320 pairs of distorted & normal fingerprints	800×750 pixels	large distortion
NIST SD27	258 pairs of latent & rolled fingerprints	800×768 pixels	low image quality, large distortion

[a] All fingerprints have a resolution of 500 ppi.

determined. In every iteration, a valid block can be with three types: fixed, undetermined and unprocessed. Fixed block means its transformation has been fixed in the last iteration, undetermined block means its transformation has not yet been fixed in the last iteration or it is a newly added block in current iteration, and unprocessed block means it has not yet been included in the current region.

Algorithm 1. Region growing MRF optimization algorithm.

Input: Valid input blocks $\{\mathbf{\Gamma}_i\}$, their corresponding blocks $\{\mathbf{\Phi}_i\}$ in reference fingerprint and their candidate transformations $\{\Upsilon_i\}$;
Output: Optimal transformation: $\Upsilon^* = \{\Upsilon^*_{i,r_i^*}\}$;

```
for ith valid block do
    Use Eq. (9) to calculate κ_i;
    if κ_i > t_r then
        |C_i = 1;
        C_i = 0;
end
D = FindLargestConnectedRegion(C);
Set D as the beginning region;
while there is any unprocessed block or the number of fixed blocks is still changed do
    Add valid 4–connected neighbors which are unprocessed to current region;
    Construct energy function Eq. (5);
    Optimize energy function using LBP and output optimal transformations Υ* = {Υ*_{i,r_i^*}} in current region;
    for each undetermined block do
        if both the similarity term and the weighted average of the compatibility term are less than t_s
           and t_c then
            |Set it as fixed block;
        end
    end
end
Υ* = {Υ*_{i,r_i^*}};
```

In every iteration, we add the valid 4-connected neighbors which are unprocessed to the current region and construct the energy function using Eq. (5). The loopy belief propagation (LBP) algorithm [28] is used to optimize the energy function. LBP was originally proposed to perform exact inference on trees. However, empirical studies have shown that it also yields good approximate results on MRF [28,29].

After LBP optimization of every iteration, we check if the solution of undetermined blocks in the current region is good enough. An undetermined block is set as a fixed block if both its similarity term and the weighted average of the compatibility term are less than predetermined thresholds t_s and t_c. $\lambda_{c,1}$ denotes the compatibility weight between the fixed block and undetermined block, and $\lambda_{c,2}$ between two undetermined blocks. The iterative algorithm continues until there is no unprocessed blocks and the number of fixed blocks does not change. The region growing process of an example is shown in Fig. 8. Note that, if the beginning region is null, LBP is directly applied to all valid input blocks.

This algorithm is summarized in Algorithm 1. It returns the globally optimal transformations of valid input blocks, namely, $\Upsilon^* = \{\Upsilon^*_{i,r_i^*}\}(1 \le r_i^* \le n_c)$, where r_i^* denotes the index of final selected candidate transformation for block $\mathbf{\Gamma}_i$. Let $\mathcal{X}$ denote the vector of center points of $\mathbf{\Gamma}$, $\mathcal{Y}$ denote the vector of center points of transformed blocks of $\mathbf{\Gamma}$ using Υ^*, respectively. Finally, a TPS model fitted from $\mathcal{X}$ to $\mathcal{Y}$ is used to register the two fingerprints. Deformation field $\mathcal{D}$ between two fingerprints can be obtained using the following formula:

$$\mathcal{D} = \mathcal{X} - \mathcal{Y}. \tag{10}$$

Fig. 9 give two examples to compare global MRF optimization algorithm with region growing MRF optimization algorithm. In the global MRF optimization algorithm, we directly use all valid blocks to construct energy function and use LBP to optimize it. From Fig. 9, we can see the region growing algorithm obtains better results.

The processes of low resolution and high resolution block matching are the same except for some parameters. Table 1 summarizes the parameters used in our experiments. Note that, these parameters are first selected based on experience and then tuned according to the experimental results of a few examples.

5. Experiment

The proposed algorithm has been evaluated in terms of registration accuracy (Section 5.1) as well as matching accuracy (Section 5.2) using three databases (see Table 2). The computational cost is discussed in Section 5.3.

5.1. Registration accuracy

We compare the registration results of three registration approaches, namely, the minutiae-based rigid registration, the initial registration step of the proposed dense registration, and the proposed dense registration. The rigid transformation model fitted to the matched minutiae obtained using the method introduced in 3.1 is used to finish the minutiae-based rigid registration. And the method introduced in Section 3 is used to finish the initial registration. Fig. 10 gives the results of three examples (the first two from FVC2004 DB1_A and the last one from TDF). From Fig. 10, we can clearly see that:

- the performance of the dense registration approach is superior to the minutiae-based rigid registration and the initial registration, especially when there exists severe distortion.
- the dense registration approach registers not only the minutiae but also the ridges, while the minutiae-based rigid registration registers only few minutiae, the initial registration registers some minutiae and some ridges.
- the matching scores between input fingerprints and the mated reference fingerprints are significantly improved after the dense registration.
- the image correlation coefficients between input fingerprints and the mated reference fingerprints in overlapping area are also significantly improved after the dense registration. Here

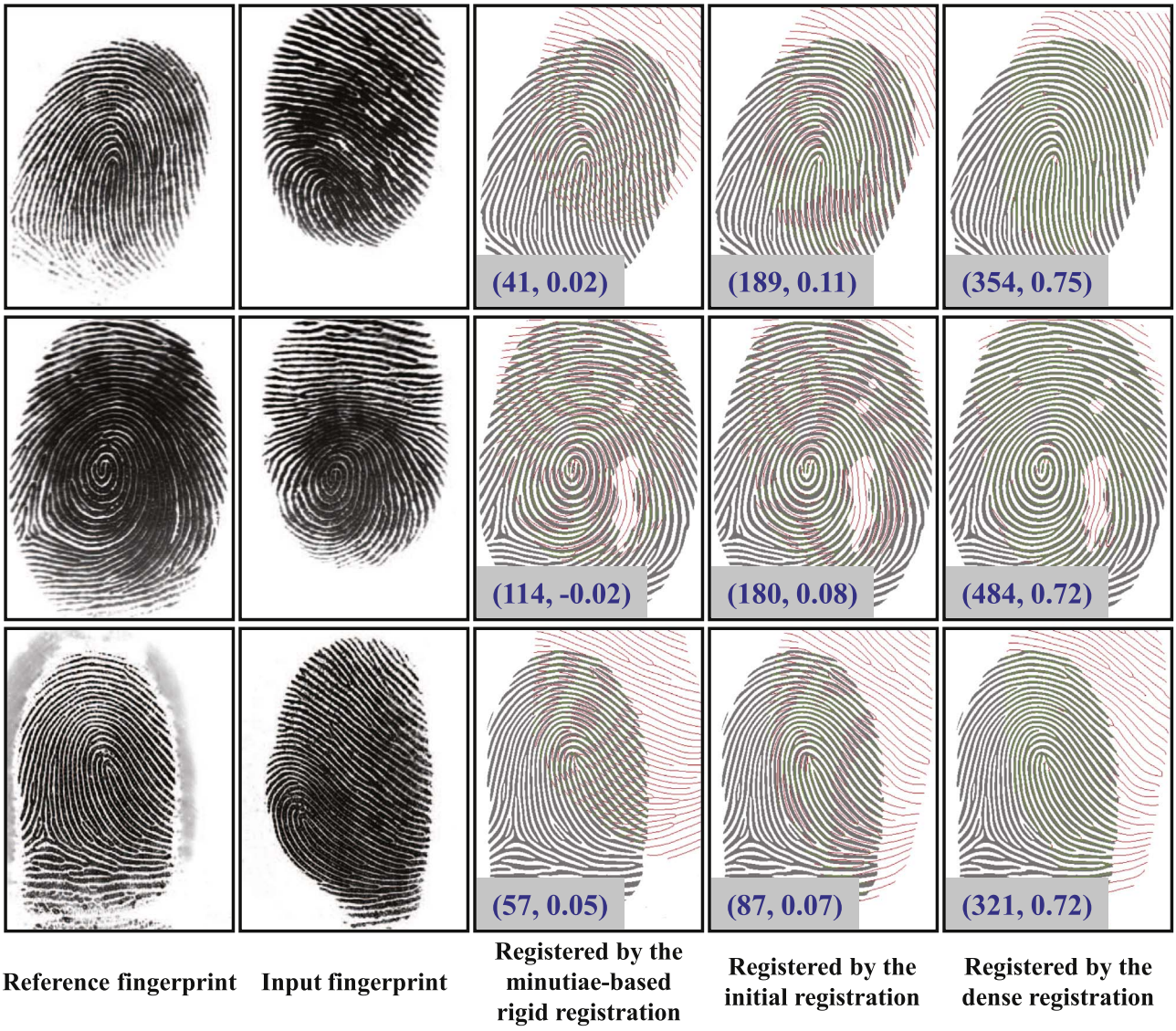

Fig. 10. Registration results by three registration approaches for three examples (the first two from FVC2004 DB1_A and the last one from TDF). The blue numbers in () are (minutiae matching score computed by VeriFinger, image correlation coefficient). We can see that the dense registration produces better registration results, leading to higher minutiae matching scores and image correlation coefficients of mated fingerprints. (For interpretation of the references to color in this figure legend, the reader is referred to the web version of this article.)

the image correlation coefficient is calculate using the same method in Eq. (9).

The above experiments were also conducted on NIST SD27, the most widely used latent fingerprint database. Note that, the latent fingerprints are first enhanced using the methods in [4]. Three examples in Fig. 11 demonstrate that the proposed algorithm is robust to image noise.

In order to directly measure the difference between automatically estimated deformation grid and ground truth, we have manually registered 120 pairs of fingerprints in TDF as ground truth. A software tool was developed to assist manual registration. Using this software, the manual registration process is as follows:

1. Initially matching minutiae found by the matching algorithm described in 3.1 are shown on the two fingerprint images.
2. A TPS model fitted to these matching minutiae is used to align the two fingerprints and the registration result (just like the images in third column of Fig. 12) is shown in another window.
3. The user adds, moves, or deletes matching minutiae or points iteratively. After each operation of the user, the registration result is updated.
4. When the user finds that the registration is sufficiently good (namely, all ridges in the overlapping area become green), the manually marked matching points are saved and the process ends.

In most cases, the number of additional point pairs is much more than the number of initially matched minutiae pairs. A pair of manually registered fingerprints are shown in Fig. 12. For scientifically and reasonably evaluating the registration algorithm, the dense grid (10×10 pixels) is used to calculate the registration error which is measured by the average distance from the ground truth. Note that, the sampling grid is only valid in fingerprint area. The registration error distributions are shown in Fig. 13 and the mean registration error of the minutiae-based rigid registration, the initial registration, and the dense registration are 23.0, 7.5, and 4.6, respectively. From Fig. 13, we can see the dense registration outperforms the minutiae-based rigid registration algorithm and the initial registration algorithm. Fig. 14 gives an example to

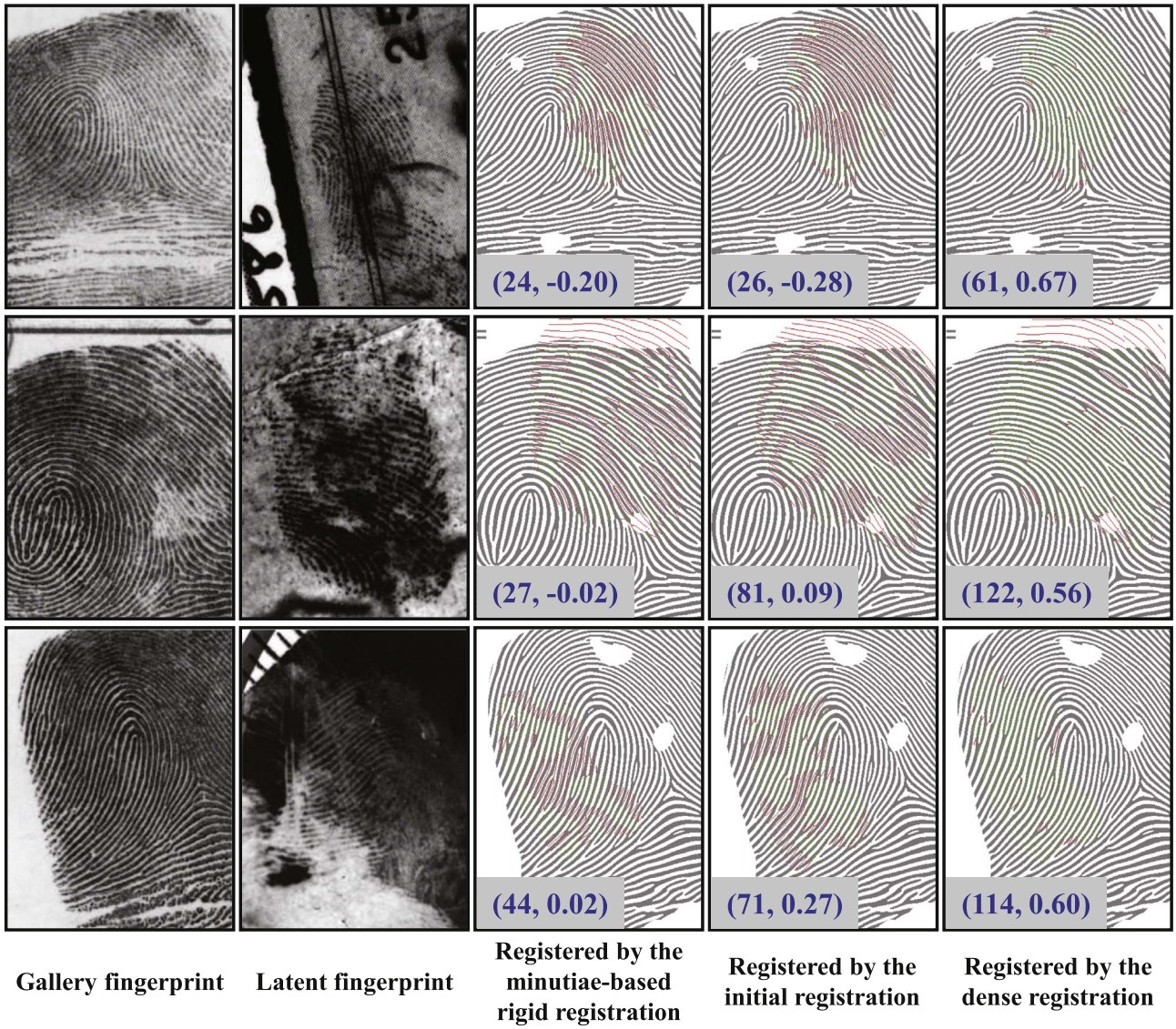

Fig. 11. Registration results by three registration approaches for three examples from NIST SD27. The blue numbers in () are (minutiae matching score computed by VeriFinger, image correlation coefficient). The dense registration improves the minutiae matching scores and image correlation coefficients of mated fingerprints. (For interpretation of the references to color in this figure legend, the reader is referred to the web version of this article.)

shown the deformation grids estimated by the three different algorithms.

Caused by complex background pattern, severe distortion, wet or dry condition etc., there may be some wrong matched minutiae in the initial registration. Fortunately, benefitting from the proposed region growing global optimization algorithm, some errors can be removed in dual-resolution block-based registration. Fig. 15 gives an example.

Although most fingerprints can be densely registered, there are some failure cases. Our analysis of failure cases shows that most of them are caused by very low image quality which leads to the badly initial registration results. Such an example is shown in Fig. 16.

5.2. Matching accuracy

Fingerprint distortion has a negative impact on genuine matches. This is one of the main reasons for the higher error rates of participating algorithms on FVC2004 DB1 than other FVC databases. To quantitatively evaluate the contribution of the dense registration algorithm to fingerprint matching, we conducted three matching experiments on FVC2004 DB1_A which is the most widely used fingerprint database for studying fingerprint distortion. There are $\frac{8\times7}{2}\times100=2,800$ genuine matches and $\frac{100\times99}{2}=4,950$ impostor matches. VeriFinger 6.2 SDK [23] was used as the fingerprint matcher. The input fingerprint pairs to VeriFinger are aligned by the three different registration algorithms, respectively. Detection Error Tradeoff (DET) curve is commonly used to report fingerprint matching performance. A DET curve plots the FMR (False Match Rate) against FNMR (False Non-Match Rate). For the same FMR, the lower FNMR indicates the higher matching performance. For this experiment, the DET curves are shown in Fig. 17(a). From Fig. 17(a), we can see that the proposed algorithm performs the best consistently.

Considering that minutiae matchers (like VeriFinger) do not fully utilize the advantage of the dense registration, we use image correlator, which outputs the image correlation coefficient, as a fingerprint matcher and test it on FVC2004 DB1_A. Fingerprint pairs aligned by the three different registration algorithms are input to image correlator. The genuine and impostor distributions of three registration algorithms are shown in Fig. 18. From Fig. 18,

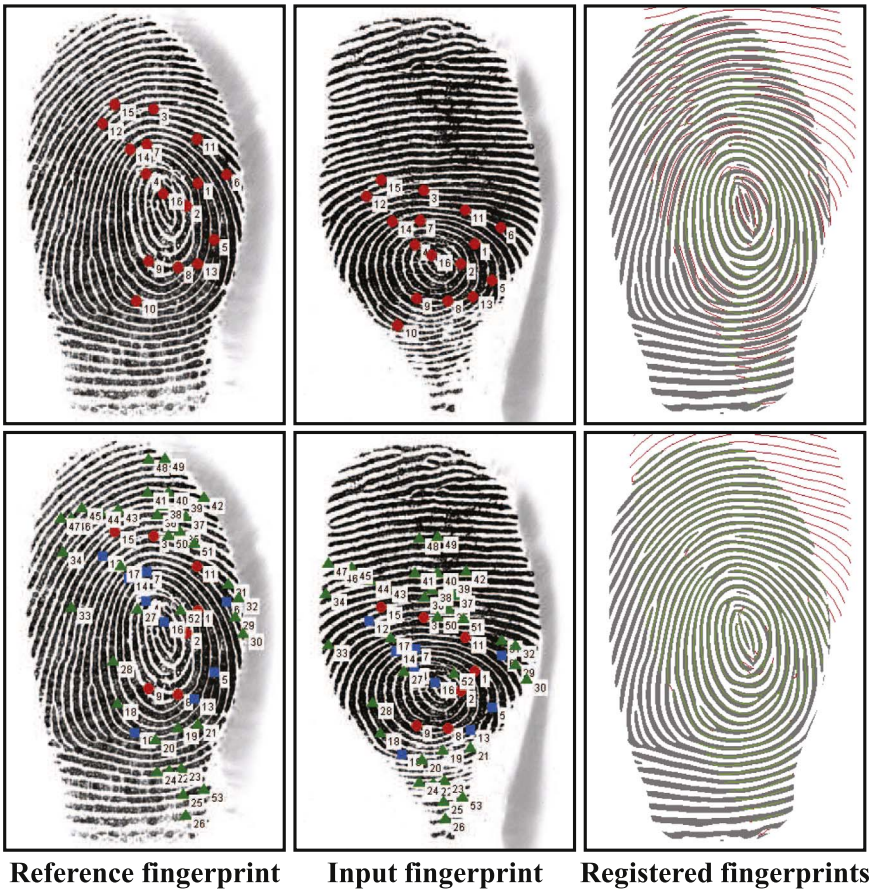

Fig. 12. A pair of manually registered fingerprints used as ground truth for quantitatively measuring registration error. The top row shows the registration result based on the initial minutiae pairs found by the minutiae matching algorithm described in 3.1. The bottom row shows the final registration result after the locations of some minutiae (blue boxes) are manually corrected and some additional point pairs (green triangles) are manually added. (For interpretation of the references to color in this figure legend, the reader is referred to the web version of this article.)

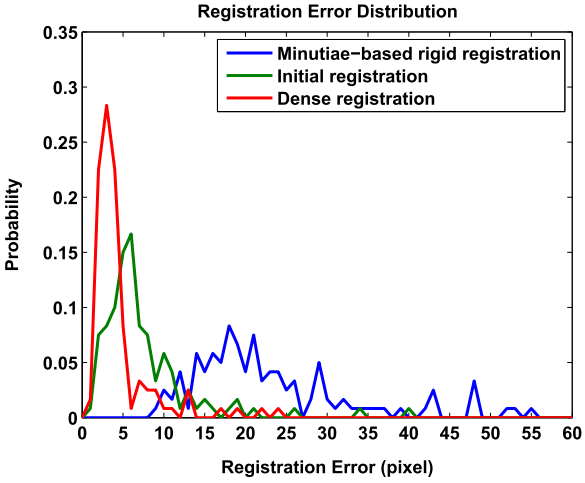

Fig. 13. Registration error distributions of three algorithms on 120 pairs of fingerprints from TDF database. The registration error is large after the minutiae-base rigid registration, while it is reduced after the initial registration and significantly reduced after the dense registration.

we can see that:

- the genuine image correlation coefficients after the initial registration are slightly improved, while the impostor image correlation coefficients do not change,
- the genuine image correlation coefficients after the dense registration are significantly improved, while the impostor image correlation coefficients are only slightly improved,
- the genuine image correlation coefficients and the impostor image correlation coefficients after the dense registration are separated greatly, while they overlap a lot after the initial registration, and they are almost totally overlapping after the minutiae-based rigid registration.

Fig. 17(b) shows the image correlation coefficient DET curves of three registration algorithms. From Fig. 17(b), we can see that the dense algorithm obtains the lowest EER (2.25%).

Minutiae matcher and image correlator are mutually complementary. Since the focus of this paper is registration problem rather than the scoring problem, we use the simple sum rule to fuse them into a new score. Since the interval of image correlation coefficient is $[-1,1]$, we use a simple min-max rule to normalize the image correlation coefficient into range $[0,1]$. For matching scores outputted by VeriFinger, we first set the matching score greater than 100-100, then use the min-max rule to normalize the matching score. Finally, the fusion score is obtained using the following formula.

$$s_f = \rho s_c + (1-\rho)s_m, \tag{11}$$

where s_f denotes the final score, s_c denotes the normalized image correlation coefficient, s_m denotes the normalized VeriFinger matching score, ρ is weight coefficient. ρ is empirically set as 0 in the minutiae-based rigid registration, 0.3 in the initial registration and 0.65 in the dense registration. The fusion DET curves are reported in Fig. 17(c). From Fig. 17(c), we can see the EER of proposed

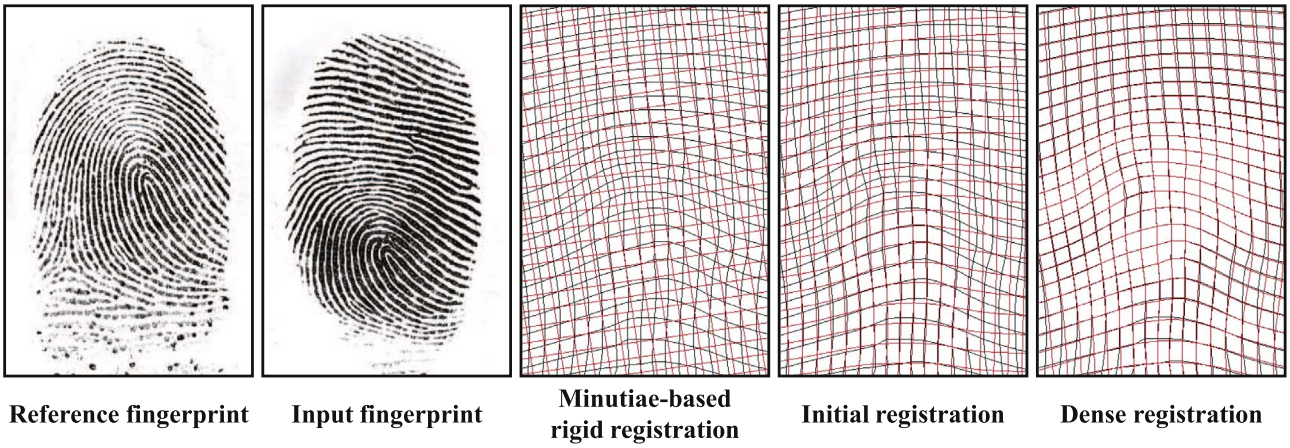

Fig. 14. Deformation grids (in red) between two mated fingerprints obtained by three different registration algorithms overlaid on the deformation grid (in black) of ground truth. For the minutiae-based rigid registration, the initial registration and the dense registration, the average distances from the ground truth (in valid area) are 21.7 pixels, 10.4 pixels and 1.4 pixels, respectively. Note that, the grids are drew with 20×20 pixels for visualization purpose.

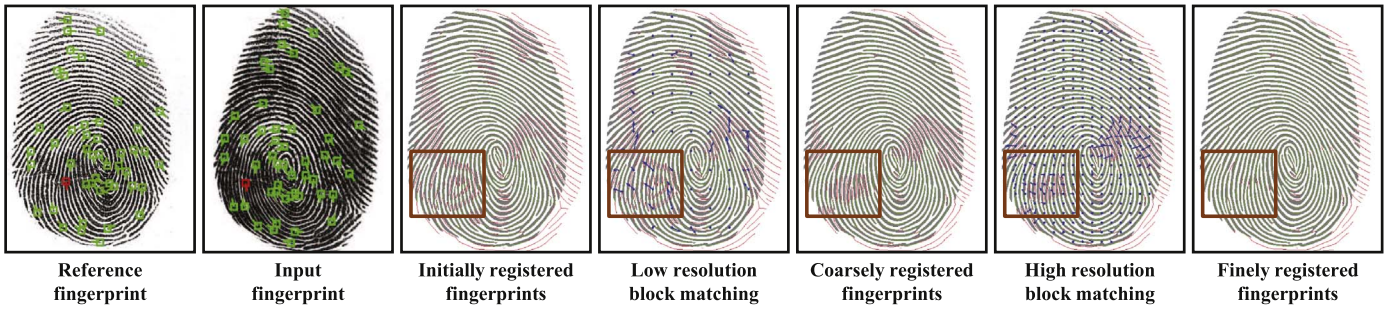

Fig. 15. The dense registration algorithm is not sensitive to wrong matched minutiae. A wrong minutiae pair is drawn in red color in the left two images. In the right five images showing the registration process, the brown box indicates the region where the initial registration error is gradually corrected. (For interpretation of the references to color in this figure legend, the reader is referred to the web version of this article.)

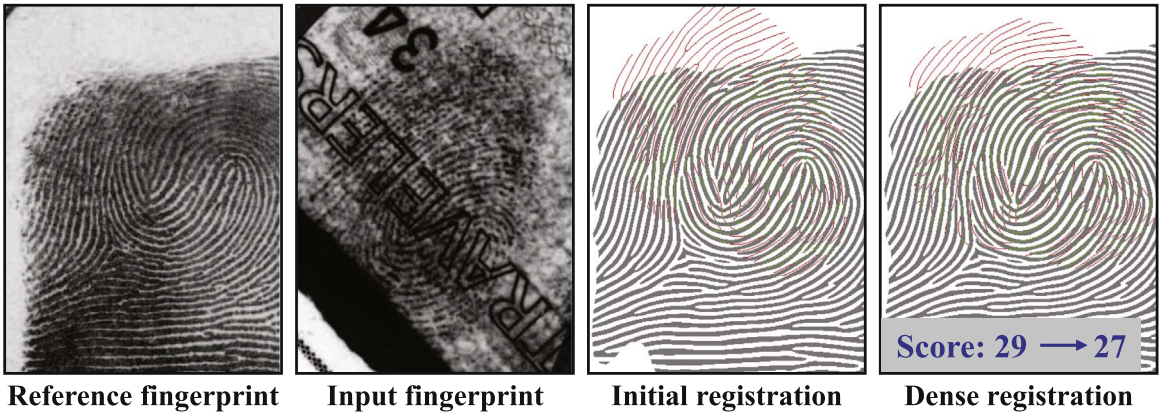

Fig. 16. A failure example of error dense registration due to low quality. The minutiae matching score slightly drops.

algorithm become more lower (0.89%), demonstrating the efficacy of the fusion.

We also compare the proposed algorithm with the top matching algorithms in FVC2004 [15]. The matching performance is summarized in Table 3. The algorithms are sorted with the ascending order of EER. From Table 3, we can see the proposed algorithm obtains the lowest EER, FMR100, FMR1000 and ZeroFMR, demonstrating the advantage of the proposed algorithm.

To further evaluate the proposed algorithm on distorted fingerprints, we also conducted experiments on TDF, which contains 320 distorted fingerprints and the corresponding 320 normal fingerprints. For TDF, the 320 pairs of fingerprints are from 185 fingers. Thus, there are 320 genuine matches and $\frac{185 \times 184}{2} = 17,020$ impostor matches. Eq. (11) is used to calculate the final score. The fusion DET curves are shown in Fig. 19. After the dense registration, the EER is significantly reduced to 0.31%, demonstrating its high performance. The summary of matching performance is reported in Table 4.

In order to further evaluate the dense registration algorithm, we conducted a matching experiment on NIST SD27 latent fingerprint database. The Cumulative Match Characteristic (CMC) curve is commonly used to report latent matching accuracy. To make the experiment more realistic, we use all 27,000 file fingerprints in the NIST SD14 database as the background database.

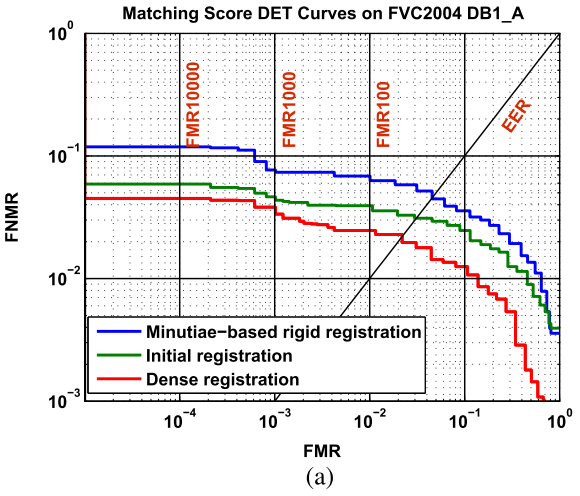

(a)

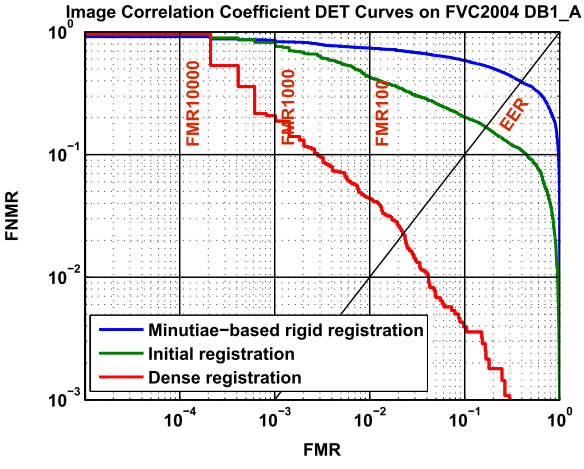

(b)

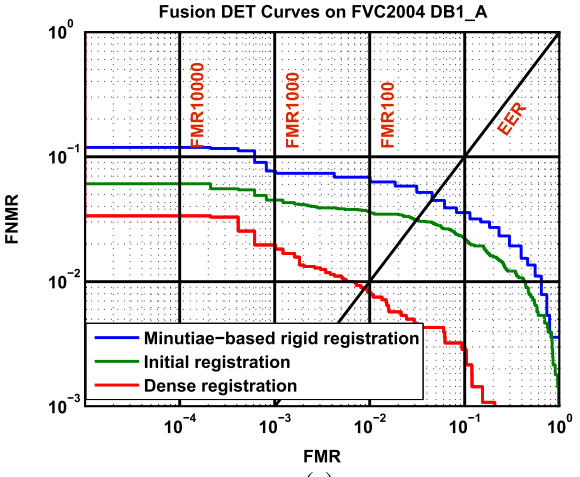

(c)

Fig. 17. DET curves of three matching score computation methods on FVC2004 DB1_A combining with three registration algorithms. The three matching score computation methods are (a) Verifinger, (b) image correlator and (c) score level fusion between (a) and (b).

Since it is very time consuming to run the registration algorithms for the whole background database, we use VeriFinger to find the top 200 candidates for each latent which is first enhanced using method in [4]. Then three registration algorithms are used to align each latent fingerprint to corresponding top 200 gallery fingerprints and matching scores between aligned fingerprints are computed using Eq. (11). From the CMC curves shown in Fig. 20, we can see that the proposed algorithm achieves the highest rank-1 rate.

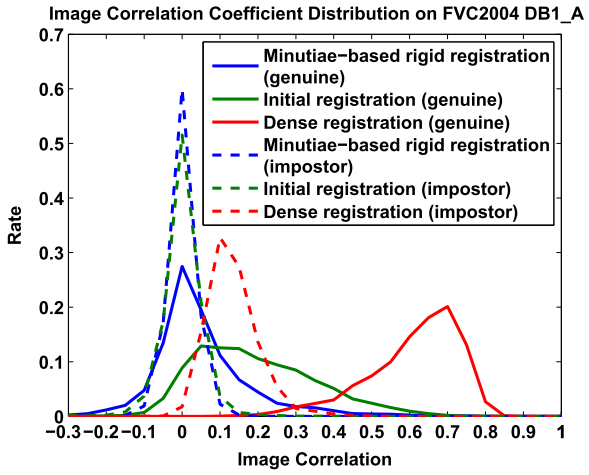

Fig. 18. Image correlation coefficient distributions of genuine and impostor by three registration algorithms on FVC2004 DB1_A. The genuine and impostor distributions are well separated by the dense registration.

Table 3
Matching performances (sorted according to EER) of proposed method and top fingerprint matchers on FVC2004 DB1_A [15].

Algorithm	EER	FMR100	FMR1000	ZeroFMR
Proposed	0.89%	0.82%	1.96%	3.36%
P047	1.97%	2.86%	4.36%	8.21%
P101	2.72%	3.86%	9.25%	13.43%
Initial registration	3.11%	3.57%	4.50%	6.07%
P097	3.38%	5.54%	9.75%	12.93%
P009	3.62%	5.54%	11.68%	15.39%
P049	3.91%	7.11%	12.43%	17.96%
Minutiae-based rigid registration	4.55%	6.86%	7.68%	11.86%

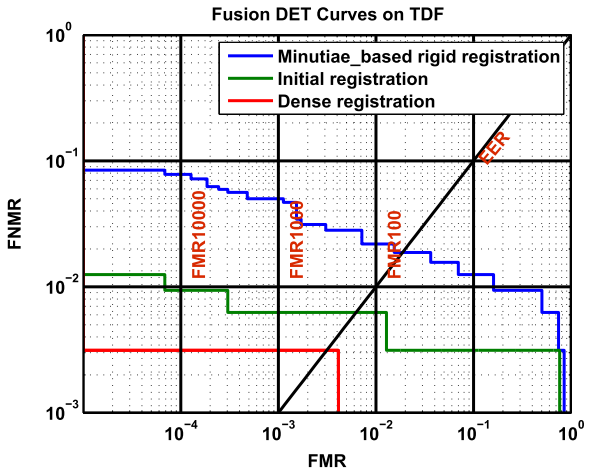

Fig. 19. Fusion DET curves on TDF using the three different registration algorithms.

Table 4
Matching performance on TDF using different algorithms.

Algorithm	EER	FMR100	FMR1000	ZeroFMR
Proposed	0.31%	0.00%	0.31%	0.31%
Initial registration	0.63%	0.63%	0.63%	1.25%
Minutiae-based rigid registration	1.88%	2.19%	5.00%	8.44%

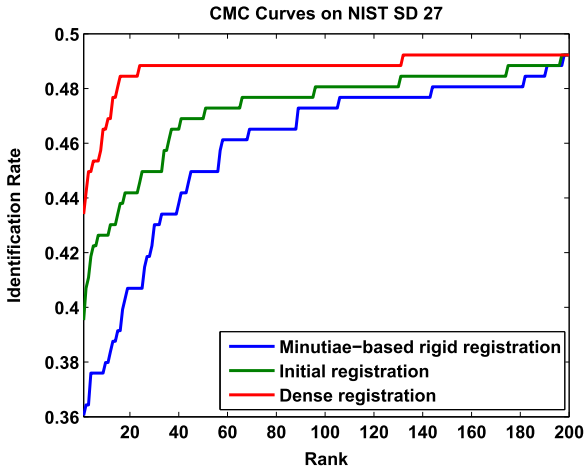

Fig. 20. The CMC curves on NIST SD27 latent fingerprint database using the three different registration algorithms. Registration is performed for top 200 candidates of each latent fingerprint.

Table 5
Speed of the proposed dense registration algorithm.

Algorithm	Time (s)		
	FVC2004 DB1	TDF	NIST SD27
Minutiae-based initial registration	0.31	0.45	0.42
Orientation&period-based initial registration	1.09	1.39	1.41
Low resolution block-based registration	1.21	1.62	1.43
High resolution block-based registration	1.64	2.31	1.82

5.3. *Efficiency*

The average times of the proposed dense registration algorithm on a PC with 2.0 GHz CPU are reported in Table 5. Initial registration is implemented in MATLAB and dual-resolution block-based registration is implemented in C. The total computational time of proposed dense registration algorithm is about 3, 4, 3 s for one fingerprint pair in FVC 2004 DB1, TDF and NIST SD27, respectively. Fingerprints in TDF need longer time due to their larger valid fingerprint area.

6. Conclusion

Elastic deformation of fingerprints poses a big challenge for dense registration of fingerprints, which is beneficial to various fingerprint matching methods. Most existing fingerprint matching algorithms can output only matched minutiae and hence cannot register severely distorted fingerprints.

In this paper, we proposed a novel dense fingerprint registration algorithm, which consists of an initial registration step and a dual-resolution block-based registration step. The dual-resolution block-based registration is approached in an energy minimization framework which consists of local search, energy function construction and global optimization. The dense registration algorithm is insensitive to wrong initially matched minutiae. Experimental results on FVC2004 DB1, TDF and NIST SD27 latent fingerprint database, whose images are markedly affected by elastic distortion, show that the proposed algorithm not only produces more accurate registration results but also improves the matching performance by fusion of minutiae matching and image correlation.

Future directions include increasing the speed of the proposed algorithm and improving the accuracy for latent fingerprints. And we will also extend the proposed algorithm to other applications, such as seamless fingerprint mosaicking [19,30].

Acknowledgments

This work is supported by the National Natural Science Foundation of China under Grants 61622207, 61373074, 61225008, 61572271, and 61527808, the National Basic Research Program of China under Grant 2014CB349304.

References

[1] D. Maltoni, D. Maio, A.K. Jain, S. Prabhakar, Handbook of Fingerprint Recognition, 2nd edition, Springer-Verlag, 2009.
[2] L. Hong, Y. Wan, A.K. Jain, Fingerprint image enhancement: algorithm and performance evaluation, IEEE Trans. Pattern Anal. Mach. Intell. 20 (8) (1998) 777–789.
[3] S. Chikkerur, A.N. Cartwright, V. Govindaraju, Fingerprint enhancement using STFT analysis, Pattern Recognit. 40 (1) (2007) 198–211.
[4] X. Yang, J. Feng, J. Zhou, Localized dictionaries based orientation field estimation for latent fingerprints, IEEE Trans. Pattern Anal. Mach. Intell. 36 (5) (2014) 955–969.
[5] K. Cao, E. Liu, A.K. Jain, Segmentation and enhancement of latent fingerprints: a coarse to fine ridge structure dictionary, IEEE Trans. Pattern Anal. Mach. Intell. 36 (9) (2014) 1847–1859.
[6] M. Liu, X. Chen, X. Wang, Latent fingerprint enhancement via multi-scale patch based sparse representation, IEEE Trans. Inf. Forensics Secur. 10 (1) (2015) 6–15.
[7] A. Senior, R. Bolle, Improved fingerprint matching by distortion removal, IEICE Trans. Inf. Syst. 84 (7) (2001) 825–831.
[8] X. Si, J. Feng, J. Zhou, Y. Luo, Detection and rectification of distorted fingerprints, IEEE Trans. Pattern Anal. Mach. Intell. 37 (3) (2015) 555–568.
[9] N. Yager, A. Amin, Evaluation of fingerprint orientation field registration algorithms, in: Proceedings of International Conference on Pattern Recognition, vol. 4, 2004, pp. 641–644.
[10] D. Wan, J. Zhou, Fingerprint recognition using model-based density map, IEEE Trans. Image Process. 15 (6) (2006) 1690–1696.
[11] J. Feng, Combining minutiae descriptors for fingerprint matching, Pattern Recognit. 41 (1) (2008) 342–352.
[12] J. Feng, Z. Ouyang, A. Cai, Fingerprint matching using ridges, Pattern Recognit. 39 (11) (2006) 2131–2140.
[13] A. Ross, S.C. Dass, A.K. Jain, Fingerprint warping using ridge curve correspondences, IEEE Trans. Pattern Anal. Mach. Intell. 28 (1) (2006) 19–30.
[14] A. Sotiras, C. Davatzikos, N. Paragios, Deformable medical image registration: a survey, IEEE Trans. Med. Imaging 32 (7) (2013) 1153–1190.
[15] FVC2004: The Third International Fingerprint Verification Competition, ⟨http://bias.csr.unibo.it/fvc2004/⟩.
[16] NIST Special Database 27, Fingerprint Minutiae from Latent and Matching Tenprint Images, ⟨http://www.nist.gov/srd/nistsd27.cfm⟩.
[17] M. Tico, P. Kuosmanen, Fingerprint matching using an orientation-based minutia descriptor, IEEE Trans. Pattern Anal. Mach. Intell. 25 (8) (2003) 1009–1014.
[18] A.M. Bazen, S.H. Gerez, Fingerprint matching by thin-plate spline modelling of elastic deformations, Pattern Recognit. 36 (8) (2003) 1859–1867.
[19] A. Ross, S. Shah, J. Shah, Image versus feature mosaicing: a case study in fingerprints, in: Proceedings of SPIE Conference on Biometric Technology for Human Identification III, 2006, pp. 620208–1–620208–12.
[20] R. Cappelli, M. Ferrara, D. Maltoni, Minutia cylinder-code: a new representation and matching technique for fingerprint recognition, IEEE Trans. Pattern Anal. Mach. Intell. 32 (12) (2010) 2128–2141.
[21] X. Cheng, S. Tulyakov, V. Govindaraju, Minutiae-based matching state model for combinations in fingerprint matching system, in: Proceedings of the IEEE Conference on Computer Vision and Pattern Recognition Workshops, vol. 13, 2013, pp. 92–97.
[22] F.L. Bookstein, Principal warps: thin plate splines and the decomposition of deformations, IEEE Trans. Pattern Anal. Mach. Intell. 11 (6) (1989) 567–585.
[23] Neurotechnology Inc., VeriFinger, ⟨http://www.neurotechnology.com⟩, 2009.
[24] M. Leordeanu, M. Hebert, A spectral technique for correspondence problems using pairwise constraints, in: Proceedings of the IEEE International Conference on Computer Vision, 2005, pp. 1482–1489.
[25] M. Kass, A. Witkin, Analyzing oriented patterns, Comput. Vis. Graph. Image Process. 37 (3) (1987) 362–385.
[26] J. Bigun, G.H. Granlund, Optimal orientation detection of linear symmetry, in: Proceedings of the First International Conference on Computer Vision, 1987, pp. 433–438.

[27] R.P. Krish, J. Fierrez, D. Ramos, J. Ortega-Garcia, J. Bigun, Pre-registration of latent fingerprints based on orientation field, IET Biom. 4 (2) (2015) 42–52.
[28] M.F. Tappen, W.T. Freeman, Comparison of graph cuts with belief propagation for stereo, using identical MRF parameters, in: Proceedings of the IEEE International Conference on Computer Vision, 2003, pp. 900–907.
[29] R. Szeliski, R. Zabih, D. Scharstein, O. Veksler, V. Kolmogorov, A. Agarwala, M. Tappen, C. Rother, A comparative study of energy minimization methods for markov random fields with smoothness-based priors, IEEE Trans. Pattern Anal. Mach. Intell. 30 (6) (2008) 1068–1080.
[30] K. Choi, H. Choi, S. Lee, J. Kim, Fingerprint image mosaicking by recursive ridge mapping, IEEE Trans. Syst. Man Cybern.– Part B: Cybern. 37 (5) (2007) 1191–1203.

Xuanbin Si received B.S. degree and Ph.D. degree from the Department of Automation, Tsinghua University, Beijing, China, in 2010 and 2015, respectively. He is now a post doctoral researcher in Graduate School at Shenzhen, Tsinghua University. His research interests include fingerprint indexing, pattern recognition and computer vision.

Jianjiang Feng is an associate professor in the Department of Automation at Tsinghua University, Beijing. He received the B.S. and Ph.D. degrees from the School of Telecommunication Engineering, Beijing University of Posts and Telecommunications, China, in 2000 and 2007, respectively. From 2008 to 2009, he was a post doctoral researcher in the PRIP lab at Michigan State University. He is an Associate Editor of Image and Vision Computing. His research interests include fingerprint recognition and computer vision.

Bo Yuan is mostly interested in Data Mining, Evolutionary Computation and Parallel Computing. He received the B.E. degree from Nanjing University of Science and Technology, China, in 1998, and the M.Sc. and Ph.D. degrees from The University of Queensland, Australia, in 2002 and 2006, respectively. From 2006 to 2007, he was a Research Officer on a project funded by the Australian Research Council at The University of Queensland. He is currently an Associate Professor in the Division of Informatics, Graduate School at Shenzhen, Tsinghua University.

Jie Zhou was born in Nov 1968. He received B.S. degree and M.S. degree both from Department of Mathematics, Nankai University, Tianjin, China, in 1990 and 1992, respectively. He received Ph.D. degree from Institute of Pattern Recognition and Artificial Intelligence, Huazhong University of Science and Technology (HUST), Wuhan, China, in 1995. From then to 1997, he served as a postdoctoral fellow in Department of Automation, Tsinghua University, Beijing, China. From 2003, he has been a full professor in Department of Automation, Tsinghua University. His research area includes computer vision, pattern recognition and image processing. In recent years, he has authored more than 100 papers in peer-reviewed journals and conferences. Among them, more than 30 papers have been published in top journals and conferences such as PAMI, T-IP and CVPR. He is an associate editor for International Journal of Robotics and Automation, Acta Automatica and two other journals. Dr. Zhou is a recipient of the National Outstanding Youth Foundation of China.